

## RESEARCH ARTICLE

# MALDI Orbitrap Mass Spectrometry Profiling of Dysregulated Sulfoglycosphingolipids in Renal Cell Carcinoma Tissues

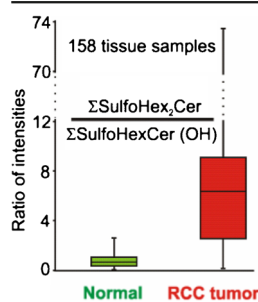
Robert Jirásko,<sup>1</sup> Michal Holčapek,<sup>1</sup> Maria Khalikova,<sup>1</sup> David Vrána,<sup>2</sup> Vladimír Študent,<sup>3</sup> Zuzana Prouzová,<sup>4</sup> Bohuslav Melichar<sup>2</sup>

<sup>1</sup>Department of Analytical Chemistry, Faculty of Chemical Technology, University of Pardubice, Studentská 573, 53210, Pardubice, Czech Republic

<sup>2</sup>Department of Oncology, Faculty of Medicine and Dentistry, Palacký University, I.P. Pavlova 6, 775 20, Olomouc, Czech Republic

<sup>3</sup>Department of Urology, Faculty of Medicine and Dentistry, Palacký University, I.P. Pavlova 6, 775 20, Olomouc, Czech Republic

<sup>4</sup>Department of Clinical and Molecular Pathology, Faculty of Medicine and Dentistry, Palacký University, I.P. Pavlova 6, 775 20, Olomouc, Czech Republic



**Abstract.** Matrix-assisted laser desorption/ionization coupled with Orbitrap mass spectrometry (MALDI-Orbitrap-MS) is used for the clinical study of patients with renal cell carcinoma (RCC), as the most common type of kidney cancer. Significant changes in sulfoglycosphingolipid abundances between tumor and autologous normal kidney tissues are observed. First, sulfoglycosphingolipid species in studied RCC samples are identified using high mass accuracy full scan and tandem mass spectra. Subsequently, optimization, method validation, and statistical evaluation of MALDI-MS data for 158 tissues of 80 patients are discussed. More than 120 sulfoglycosphingolipids containing one to five hexosyl units are identified in human RCC samples based on the systematic study of their fragmentation behavior. Many of

them are recorded here for the first time. Multivariate data analysis (MDA) methods, i.e., unsupervised principal component analysis (PCA) and supervised orthogonal partial least square discriminant analysis (OPLS-DA), are used for the visualization of differences between normal and tumor samples to reveal the most up- and downregulated lipids in tumor tissues. Obtained results are closely correlated with MALDI mass spectrometry imaging (MSI) and histologic staining. Important steps of the present MALDI-Orbitrap-MS approach are also discussed, such as the selection of best matrix, correct normalization, validation for semiquantitative study, and problems with possible isobaric interferences on closed masses in full scan mass spectra.

**Keywords:** Renal cell carcinoma, MALDI, Orbitrap mass spectrometry, Sulfoglycosphingolipids, Sulfatide

Received: 17 January 2017/Revised: 24 February 2017/Accepted: 25 February 2017/Published Online: 30 March 2017

## Introduction

Sulfoglycosphingolipids (glycosphingolipid sulfates or sulfatides) are acidic sphingolipids characterized by a hydrophobic ceramide lipid backbone attached to a polar saccharide chain composed of at least one anionic sulfate ester group

[1]. Sulfoglycosphingolipids are distributed in various tissues, including brain, kidney, and gastrointestinal tract, and they play major roles in signal transduction, cell adhesion, modulating growth, hormone or cytokine receptors, antigen recognition, renal ammonium excretion, and other biological functions [2, 3]. Abnormal metabolism of glycosphingolipid sulfates is associated with various diseases. Expression changes in sulfoglycosphingolipids concentrations have been reported in association with chronic metabolic acidosis [3], metachromatic leukodystrophy [4], Alzheimer's disease [5, 6], and in numerous malignant disorders, including RCC, colon, lung, and ovarian carcinomas [2, 7–10]. The majority of studies focused

**Electronic supplementary material** The online version of this article (doi:10.1007/s13361-017-1644-9) contains supplementary material, which is available to authorized users.

Correspondence to: Robert Jirásko; e-mail: robert.jirasko@upce.cz

on the analysis of galactosylceramide-1<sup>3</sup>-sulfates, the most common type of sulfoglycosphingolipids containing one hexosyl unit. Differences in the length, the degree of unsaturation, the hydroxylation of N-linked fatty acyl and sphingoid base in the ceramide part, and the number of hexosyl and sulfate units in the saccharide part result in a large structural diversity of sulfoglycosphingolipids.

These structural features cannot be distinguished by immunochemical or chromatographic methods; therefore, the utilization of mass spectrometry (MS) is essential for this type of analysis [11–13]. MS can bring the information about molecular weights of compounds of interest, however, mass spectra of lipids are very complex. Matrix interferences and isobaric overlaps of many lipid species can be present for one nominal mass, and the use of MS analyzer with high mass resolving power, high mass accuracy, and MS/MS capability is usually necessary to distinguish them [14]. Another important step is the selection of a suitable ionization technique. Electrospray ionization (ESI) is the most common ionization technique for lipid analysis and has been applied in many cases in liquid chromatography-mass spectrometry or shotgun MS analysis of sulfatides [5, 11, 15–17]. However, matrix-assisted laser desorption/ionization mass spectrometry (MALDI-MS) with 9-aminoacridine (9-AA), moderately strong base matrix enabling a selective formation of deprotonated molecules for compounds with acidic character in the negative-ion mode [18–20], has also been frequently used for analysis of sulfatides, and compared with ESI resulted in higher sensitivity and selectivity [18]. Moreover, MALDI mass spectrometry imaging (MALDI-MSI) can bring additional information about the spatial distribution of these lipids in studied tissue samples [21, 22]. MALDI-MS is also useful in the characterization of complex sulfoglycosphingolipids containing two and even more hexosyl units [13, 19, 22, 23]. Systematic MALDI-MSI study of mouse kidney resulted in the detection and spatial localization of several complex lactosylceramide-II<sup>3</sup>-sulfates and gangliotetraosylceramide-II<sup>3</sup>, IV<sup>3</sup> bis-sulfate [13, 22, 23]. Sulfoglycosphingolipids up to three hexosyl units were found in different rat organs [19]. Analytical characterization of sulfatides, major acidic glycosphingolipids in the kidney, is important, especially in human tissue samples because their concentration changes can be correlated with various diseases, as described above. The measurement of many clinical samples is necessary to consider both analytical and biological variability.

RCC is the most common type of kidney cancer in adults. RCC incidence and the mortality rate have been increasing globally during the last decade [24–27]. The major RCC histologic subtypes are clear cell (>75%), papillary (≈15%), and chromophobe (≈5%). Many studies reported enhanced activity of sulfotransferase and, consequently, elevated level of sulfatation in human RCC samples (tissue and cell lines) based on immunochemical analyses without MS application [8, 9, 28]. In contrast, MALDI-MS comparison of 59 RCC and 24 adjacent normal tissue samples reported decreased concentration of C24 and C22 hydroxylated monohexosyl sulfatides in

RCC tumor tissue, but the authors described only a low number of sulfatides and did not study complex species containing more hexosyl units [29].

In the present study, ultrahigh-resolution MALDI-Orbitrap-mass spectrometry in the negative-ion mode was used to identify as many sulfoglycosphingolipid molecular species as possible and to semiquantify those over a wide range of concentrations in RCC tumor and autologous normal tissues obtained from 80 patients. MDA was performed for all studied tissue extracts in order to visualize most significant changes in sulfoglycosphingolipid profiles between tumor and autologous normal tissue sections, and the results were compared with the data previously reported in the literature.

## Experimental

### *Preparation of Mixtures of Internal Standards*

Internal standards (IS), i.e., phosphatidic acid (PA) 14:0/14:0, phosphatidylglycerol (PG) 14:0/14:0, phosphatidylethanolamine (PE) 14:0/14:0, phosphatidylcholine (PC) 14:0/14:0, phosphatidylinositol (PI) 8:0/8:0, phosphatidylserine (PS) 14:0/14:0, sphingomyelin (SM) d18:1/12:0, and SulfoHexCer d18:1/12:0 were purchased from Avanti Polar Lipids (Alabaster, AL, USA) and used for the validation and semiquantitation MALDI-MS experiments. Stock solutions of individual IS were prepared in a mixture of chloroform and 2-propanol (1:4, v/v). Two IS mixtures were subsequently prepared for validation and semiquantitative experiments. IS mixture 1, used for the preparation of calibration solutions, was prepared by mixing of 8 μL of each IS. The ratio of IS used for the preparation of the second IS mixture 2 as well as the concentration of stock solutions are listed in the Supplementary Table S1.

### *RCC Tissue Samples and Their Extraction*

Eighty kidney tumor and 78 autologous normal kidney tissue samples from 80 RCC patients (see Table 1) were obtained from the Department of Urology, Palacký University, Faculty of Medicine and Dentistry and University Hospital, Olomouc, Czech Republic. The study was approved by the Hospital Ethical Committee, and all patients signed informed consent. Tissues were obtained during surgery, immediately frozen, and stored at –80 °C until sample processing and analysis. Extracts of human kidney tissues were prepared by modified Folch method with chloroform-methanol-water mixture. Briefly, 25 mg of kidney tissue and 17.5 μL (6 μL for low concentration level and 24 μL for high concentration level in case of validation experiments) of IS mixture 2 were ultrasonicated with 6 mL of chloroform-methanol (2:1, v/v) mixture. The homogenate was mixed with 120 μL of water and centrifuged at 3000 rpm for 5 min at room temperature. The bottom chloroform layer containing lipids was evaporated by a stream of nitrogen and redissolved in 0.5 mL of chloroform-2-propanol mixture (1:1, v/v). Samples were finally diluted four times in methanol before the mixing with MALDI matrix solution.

**Table 1.** Clinicopathological characteristics of RCC tissue samples (80 patients)

Number of tissues		Patients		Histological type of tumor	
Normal	78	Age range	18–81 y	Clear cell	71 (89%)
RCC	80	Age median	66 y	Papillary	5 (6%)
Male	75%	BMI range	17.9–54.5	Chromophobe	2 (3%)
Female	25%	BMI median	27.5	Oncocytic adenoma	1 (1%)
				Ewing sarcoma	1 (1%)
Tumor stage (number of individual patients)					
Not classified	pT1aNxMx (5), pT1bNxMx (5), pT2aNxMx (4), pT2bNxMx (2), pT3aNxMx (13)				
I	pT1aN0M0 (8), pT1bN0M0 (14)				
II	pT2aN0M0 (5), pT2bN0M0 (1)				
III	pT3aN0M0 (11), pT3aN1Mx (2), pT3bN0M0 (1), pT3aNxM0 (1)				
IV	pT2bNxM1 (1), pT3aNxM1 (3), pT3aN1M1 (2)				

### Method Validation

A pooled sample was prepared from 20 randomly selected patients containing tumor and autologous normal tissue samples equally. Validation parameters were studied according to “Guideline on bioanalytical method validation” by European Medicines Agency [30] and included the following parameters: selectivity, calibration curve, within-run and between-run precision, carry-over effect, and freeze/thaw stability. Linearity range, limit of detection (LOD), and limit of quantitation (LOQ) of developed MALDI-MS method were determined using a pooled sample of kidney tissues spiked with IS mixture 1, extracted, and then diluted with methanol to provide the final concentration listed in Supplementary Table S2. Linearity was determined from calibration curves of individual IS plotted as peak abundances against concentrations of standard solutions and fitted by linear regression. LOD and LOQ were determined from signal-to-noise ratios 3 and 10, respectively. Selectivity of tested IS was verified based on the preliminary measurement of six different tissue extracts without the addition of IS. For validation of within-run precision, three consecutive extractions of pooled RCC tissue extract with IS were performed in both high and low concentration levels and measured within 1 d. Between-run precision was determined based on the measurement of nine RCC tissue extracts with IS of high concentration level (six extracts were prepared in 1 d and three were prepared the next day). Precision was calculated taking into account mean value and standard deviation. Data are expressed as relative standard deviation (% RSD). Measurement of high number of samples with five repetitions is not possible within one run on one MALDI plate. The washing step of the plate is necessary before the next run; thus, the carry-over effect should be determined to verify efficiency of the washing procedure. Carry-over effect was determined from the blank sample, which was spotted on the washed MALDI plate on the same positions as previously measured calibration standards at the upper limit of quantitation. Freeze/thaw stability was determined for pooled sample with IS of high concentration level after two freeze/thaw cycles involving the storage of sample at  $-20\text{ }^{\circ}\text{C}$  overnight and its thawing at room temperature for 1 h. Reproducibility of spotting was calculated as the standard deviation from five consecutive spots of the sample. All validation parameters were calculated using Microsoft Excel 2010.

### Histologic Staining

Fresh tissue obtained from surgical resections was cut at  $5\text{ }\mu\text{m}$  thickness using Leica CM1950 cryostat microtome (Leica Microsystems, Wetzlar, Germany) and stained with hematoxylin and eosin (H&E) as described elsewhere [31]. Adjacent tissue slides of  $10\text{ }\mu\text{m}$  thickness were obtained and subsequently subjected to MALDI-MSI experiments.

### MALDI-Orbitrap-MS Study

Mass spectra were measured using ultrahigh-resolution MALDI mass spectrometer LTQ Orbitrap XL (Thermo Fisher Scientific, Waltham, MA, USA) equipped with the nitrogen UV laser ( $337\text{ nm}$ ,  $60\text{ Hz}$ ) with a beam diameter of about  $80\text{ }\mu\text{m} \times 100\text{ }\mu\text{m}$ . The LTQ Orbitrap instrument was operated in negative-ion mode over a normal mass range  $m/z$  400–2000; the mass resolution was set to  $R = 100,000$  (full width at half maximum definition, at  $m/z$  400) for all full scan mass spectra experiments (identical setting was used for MALDI-MSI experiments). 9-AA (Sigma-Aldrich, St. Louis, MO, USA) was dissolved in methanol (Sigma-Aldrich)-water mixture (4:1, v/v) to provide a concentration of  $5\text{ mg/mL}$ , and mixed with particular diluted tissue extracts (1:1, v/v). Deionized water was prepared with a Milli-Q Reference Water Purification System (Molsheim, France). Dried droplet crystallization was used for the sample deposition on the target plate. The deposited amount of samples was  $1.5\text{ }\mu\text{L}$ . Each sample (spotted matrix and tissue extract mixture) was prepared five times and measured in negative polarity mode. The zig-zag sample movement with  $250\text{ }\mu\text{m}$  step size was used during the individual data acquisition. The laser energy corresponded to 15% of maximum, and two microscans/scan with two laser shots per microscan at 36 different positions were accumulated for one measurement to achieve a reproducible signal. For tandem mass spectrometry (MS/MS), the isolation width  $\Delta m/z$  1, normalized collision energy from 25% up to 80%, activation Q value 0.250, activation time 30 ms, and helium as the collision gas were used for collision-induced dissociation (CID) experiments in LTQ linear ion trap. For pulsed Q collisional induced dissociation (PQD), normalized collision energy 35%, activation Q value 0.7, and activation time 0.1 ms were applied. For

higher energy collisional induced dissociation (HCD), normalized collision energy from 25% up to 50% was applied.

### *MALDI-Orbitrap-MSI Experiments*

Each tissue slice for the imaging experiments was immediately thaw-mounted onto stainless or microscopic glass plate and placed on the bottom side of sublimation condenser. The 9-AA matrix deposition was performed in a modified sublimation apparatus described previously [14] (Chemglass Life Science, Vineland, NJ, USA) with a constant vacuum of 0.04 mbar. Stable vacuum was obtained using the rotary pump Edwards E2M28 (Edwards, Crawley, UK) supplemented with the solenoid valve DN15 (Vacuubrand, Wertheim, Germany) and controlled by the vacuum controller CVC 3000 (Vacuubrand). Sublimation time was 10 min and temperature obtained in oil bath was 190 °C, respectively. All experiments were performed with the automatic gain control turned off to achieve an identical number of laser shots for each pixel. The step size of the sample was set to 120 µm. Four microscans were summed for each mass spectrum (each pixel). Mass spectrometric images were generated using tissue imaging visualization software ImageQuest 1.0.1 (Thermo Fisher Scientific).

### *Statistical Data Analysis*

MDA was performed using PCA and OPLS methods in the SIMCA software, ver. 13.0 (Umetrics, Umeå, Sweden). Data were preprocessed before statistical analysis using Pareto scaling and logarithm transformation. Box plots were calculated using Microsoft Excel 2010 and the distribution of results described using median, minimum, maximum, and variability of data sets in the first and third quartiles.

### *Lipid Nomenclature*

The lipid nomenclature used in this article is based on officially accepted terms, and builds upon the LIPID MAPS system [32] and the shorthand notation for lipid structures [33]. Although the abbreviations for most of the lipids are well defined there, the shorthand notation for sulfoglycosphingolipid species is missing. Considering that structures of these compounds are closely related to their neutral glycosphingolipid analogues, such as glucosyl, galactosyl, or lactosyl ceramide species, and the difference in the additional sulfate group in the saccharide part of molecule only can be found, we used the similar abbreviation for them and added only Sulfo- prefix indicating the presence of sulfate group. In the following text, our sulfoglycosphingolipid shorthand notification is briefly described on the example of SulfoHex<sub>2</sub>Cer 36:1 for a better understanding. The Sulfo- prefix indicates the presence of one sulfate group, the abbreviation Hex means presence of hexosyl unit without specification of stereochemistry, and additional subscript gives the information on their number (in our example two hexosyl units) on ceramide (Cer) backbone. Subsequently, the colon separating numbers 36:1 provides the information on the total number of carbon atoms and double bonds (CN:DB) of N-

linked fatty acyl and sphingoid base of ceramide part, and this annotation is based on the common assumption of a sphingoid base with two hydroxyl groups and no hydroxylation of N-acyl. In case of presence of additional hydroxyl on the ceramide part without any specification of its position, the OH in parentheses is space separated and placed behind the ceramide DB number, e.g., SulfoHex<sub>2</sub>Cer 36:1 (OH). If the type of sphingoid base and linked N-acyl is known from tandem mass spectra, the fatty acyl/alkyl level notation is applicable [33]. The hydroxylation of N-acyl part, the positions of which in the acyl chain are not known, is shown after the number of double bonds separated by an underscore. The sphingoid backbone is annotated by the number of hydroxyl groups in the sphingoid base using small letter in front of CN:DB (d for di, t for tri) and separated by a slash from the number of CN:DB of the N-linked fatty acyl, i.e., d18:1/18:0\_OH for N-acyl hydroxylation and dihydroxylated sphingoid base, t18:0/18:1 for trihydroxylated sphingoid base, and no hydroxylation of N-acyl or t18:0/18:1\_OH in case of additional hydroxylation of both parts of ceramide. For sulfoglycosphingolipids containing more than two hexosyl units, the presence of N-acetylhexoseamine (HexNAc) is typical and HexNAc abbreviation is placed between Sulfo prefix and Hex<sub>n</sub> in their shorthand notation, i.e., SulfoHexNAcHex<sub>3</sub>Cer (sulfoglycosphingolipid composed from one sulfate group, three hexosyls, and one N-acetylhexoseamine in the saccharide part).

## **Results and Discussion**

Preliminary tests and comparison with other matrices showed a good agreement with the literature [18], and 9-AA was evaluated as the best matrix for the analysis of acidic lipids. Another important step was the optimization of solvent composition to minimize the sample spreading and thus achieve the homogeneous crystallization yielding better reproducibility and increased sensitivity. The best results were obtained by dissolving the matrix in the mixture of methanol-water (4:1, v/v). The deposition of small aliquot of chloroform on MALDI plate spots before the application of diluted extract/matrix mixture completely reduced the drop spreading. All preliminary experiments, lipid identification for database creation, and subsequent validation for semiquantitative measurement were done on the pooled RCC sample.

### *Problem with Mass Interferences*

One of the most important steps is correct lipid identification and verification that identified lipids are not influenced by closed masses, which could further distort quantitative data. The basicity of 9-AA allows the formation of deprotonated molecules for polar lipid species containing acidic proton, such as phospholipid or acidic sphingolipid species. More than 600 ions corresponding to lipid species were matched with theoretical suggestions in the RCC pooled sample. Among these



phospholipids (PA, PE, PG, PI, PS, cardiolipins, and corresponding lyso species), sphingolipids (ceramide phosphate (CerP), SM, sulfatides, and gangliosides), and sterol sulfates were identified. Although a relatively high number of lipids was matched using various identification software, such as MS Analysis Tools on LipidMaps [34] or LipidXplorer [35], the problem with lipid overlaps has to be considered in case of measurement of only full scan mass spectrum without any separation step or MS shotgun approaches. Overlaps of isotopic envelopes of lipids is often present in complex biological samples and the application of mass analyzer with high resolving power or isotopic correction for lower resolution MS is required. The identification of overlapped lipids can be done based on additional MS/MS spectra measurements, where product ions corresponding to all precursors are present. However, this is not sufficient for quantitative studies of lipids, where only ion intensities from full scan mass spectra are compared. Supplementary Table S3 summarizes possible overlaps for isotopes of particular lipid species in negative-ion mass spectra. The high mass accuracy and high resolution Orbitrap-MS allow better detection of closed masses, distinguishing isobaric interferences and thus higher coverage and identification confidence of studied lipids. The application of Orbitrap XL analyzer with the resolution 100,000 (at  $m/z$  400) is sufficient to distinguish many interfering ions, but not in all cases. 9-AA matrix provides abundant  $[M - CH_3]^-$  ions of phosphatidylcholines, which are of identical  $m/z$  values as deprotonated molecules of phosphatidylethanolamines corresponding to fatty acyl composition differing by  $C_2H_4$  from PC (e.g., demethylated PC 38:4 is equal to deprotonated PE 40:4). Erroneous assignment of PC as PE species can occur and the quantitation of these species cannot be done without the previous separation step in negative-ion MALDI mass spectra of complex biological samples containing phospholipids with a significant PC content, as described previously [36]. Another problem is that product ions of PC and SM, observed even in negative-ion full scan mass spectrum, are of identical  $m/z$  values as deprotonated molecules of PA and CerP. In addition, ions corresponding to PA species largely yield from PS after ion source elimination of serine moiety ( $\Delta m/z$   $C_3H_5NO_2$ ) in negative-ion MS mode. A similar situation can be observed for all deprotonated molecules of lysophospholipid species that are of identical  $m/z$  values as product ions of their phospholipid analogues. Despite the fact that the fragmentation of precursor ion in full scan mass spectrum can be minor, lipids on these masses should not be used in quantitative studies, in order to avoid positive false results. All these problems have to be considered in MALDI-MS or ESI-MS in which only intensities from full scan mass spectrum are compared for relative or absolute quantitation. Regarding the above mentioned problems and preliminary data from MSI, we focused mainly on the analysis of sulfoglycosphingolipids (sulfatides), which showed the highest differences between tumor and normal tissue parts. Manual control of possible overlaps for all studied samples was performed after data processing to avoid problems with possible interferences.

### Identification of Sulfoglycosphingolipid Species

This section summarizes the gas-phase fragmentation processes used for the elucidation of the structure of observed glycosphingolipid sulfates. As described in the Introduction, these compounds can differ in the composition of the ceramide anchor part and the number of sulfates or hexosyl units in the saccharide part. In studied samples of RCC tissues, glycosphingolipid sulfates species containing from one up to five hexosyl units and one sulfate group were encountered. The total CN:DB number of N-linked fatty acyl and sphingoid backbone in the ceramide part were predicted even from high mass accuracy full scan mass spectra. In total, 52 species for sulfoglycosphingolipids with one, 40 with two (48 in case of fatty acyl level), 12 with three, 5 with four, and 10 with five hexosyl units were identified with mass error below 3 ppm in mass spectra of studied RCC tissue samples (Supplementary Tables S4–S6). The application of MS/MS was necessary for the determination of sulfate position or particular composition of ceramide part. Most important product ions and neutral losses (NL) observed in CID MS/MS of deprotonated molecules of all identified sulfoglycosphingolipids containing two up to five hexosyl units (including species recorded here for the first time) are listed in Supplementary Tables S5 and S6. Examples of their tandem mass spectra are shown in Figure 1. Some ions of more complex sulfoglycosphingolipids with several hexosyl units were close to LOD in the pooled sample. These low abundant ions were only added to our database for subsequent automatic collection of their intensities for all studied samples. Fragmentation was performed additionally in samples where they were of higher abundance to obtain relevant MS spectra. The fragmentation of sulfatides containing only one hexose is described elsewhere [11, 37], but the systematic fragmentation study of sulfatides containing more hexose units has not been described so far. Three types of fragmentations, CID, PQD in the linear ion trap, and HCD in the HCD cell, can be performed with LTQ XL Orbitrap configuration [38]. Supplementary Figure S1 illustrates three graphs of dependence of fragmentation efficiency on used collision energy for selected glycosphingolipid sulfates ( $m/z$  1050, 1066, and 1595). The application of collision energy (at least 30% of maximum) was necessary to start the fragmentation process, but usually energy higher than 60% of maximum was used to provide sufficient intensity of product ions required for the identification of studied glycosphingolipid sulfates.

### Fragmentation of SulfoHex<sub>2</sub>Cer

The colored arrows in all fragmentation schemes or NL and ion masses in MS/MS spectra in Figures 1, 2 and 3, Supplementary Figures S2–S5, and Supplementary Tables S5 and S6 are associated with the fragmentation processes related to particular parts of studied sulfoglycosphingolipids, where red represents NL and ions of saccharide part, green represents NL of N-acyl part, and blue represents NL of sphingoid base part. Figure 1a–c show a comparison of MS/MS for deprotonated SulfoHex<sub>2</sub>Cer d18:1/24:1 at  $m/z$  1050. As illustrated in

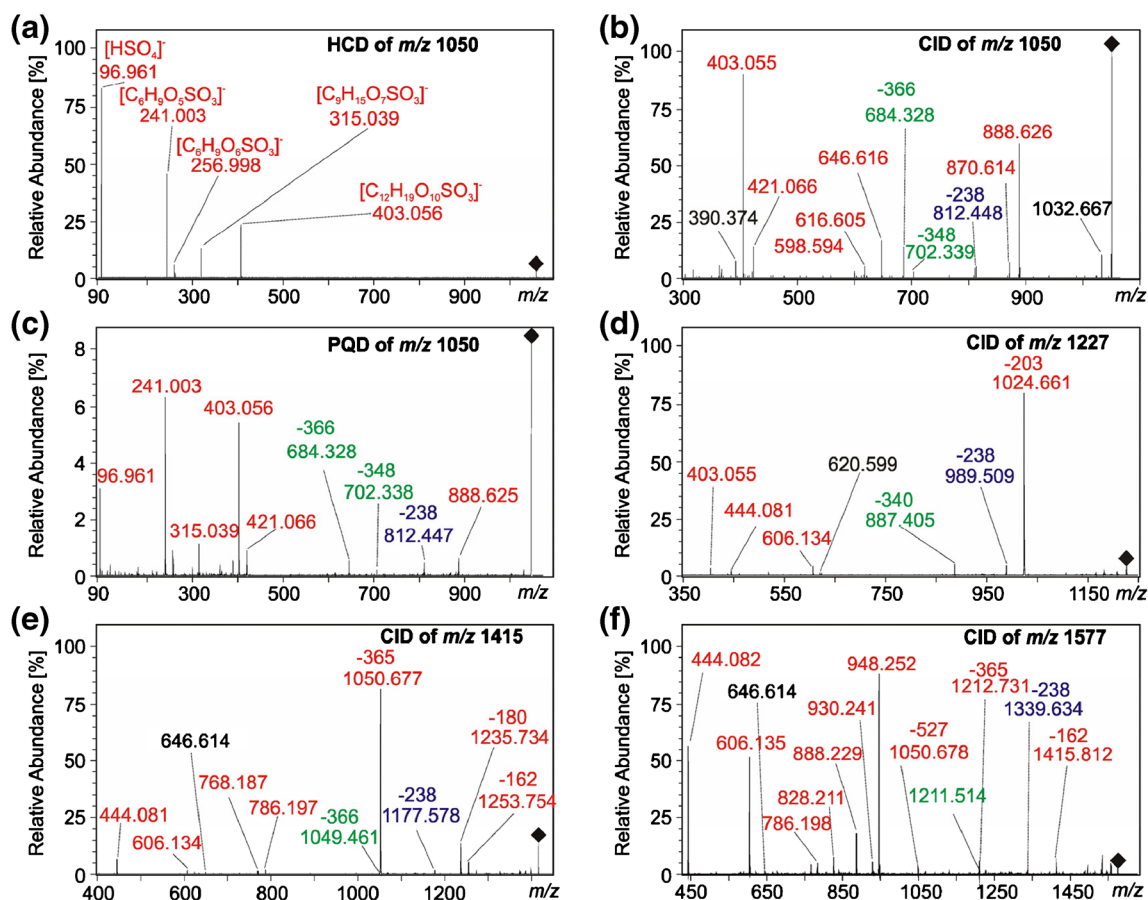


**Figure 1.** MS/MS spectra of selected sulfoglycosphingolipids: **(a)** HCD (collision energy 50%), **(b)** CID (collision energy 80%), **(c)** PQD (collision energy 35%) of deprotonated molecule of SulfoHex<sub>2</sub>Cer d18:1/24:1 at *m/z* 1050, **(d)** CID (collision energy 80%) of SulfoHexNAcHex<sub>2</sub>Cer d18:1/22:0 at *m/z* 1227, **(e)** CID of SulfoHexNAcHex<sub>3</sub>Cer d18:1/24:1 at *m/z* 1415 (collision energy 60%), and **(f)** CID (collision energy 80%) of SulfoHexNAcHex<sub>4</sub>Cer d18:1/24:1 at *m/z* 1577. The color of NL and product ions is associated with fragmentation processes related to particular parts of studied sulfoglycosphingolipids, where red represents NL and ions of saccharide part, green represents NL of N-acyl part, and blue represents NL of sphingoid base part

Figure 1a, the HCD fragmentation is dominated by product ions in low mass region, where three abundant ions at *m/z* 97 [HSO<sub>4</sub>]<sup>-</sup>, *m/z* 241 [C<sub>6</sub>H<sub>9</sub>O<sub>5</sub>SO<sub>3</sub>]<sup>-</sup>, and *m/z* 403 [C<sub>12</sub>H<sub>19</sub>O<sub>10</sub>SO<sub>3</sub>]<sup>-</sup>, together with several ions (*m/z* 315, 259, and 257) of lower intensity are present. Suggested structures of all these ions originating from saccharide part are shown in the fragmentation scheme based on CID fragmentation approach in Figure 2. On the other hand, ions in low mass region are missing in CID fragmentation (Figure 1b) due to low-mass cutoff of ion trap, and these ions are present only in additional multistage mass spectra of particular product ions. The presence of saccharide part can be inferred only from *m/z* 403 and from NL of  $\Delta m/z$  404 obtained from the same fragmentation process yielding deprotonated ceramide at *m/z* 646. Similarly as for monohexosyl sulfatides [11], important ions providing information on fatty acyl length of N-acyl at *m/z* 702 (NL of fatty acyl chain as a ketene via the NH-CO bond cleavage), *m/z* 684 (NL of ketene and additional loss of water), sphingoid base at *m/z* 812 (NL of sphingoid base as aldehyde), and *m/z* 810 (812-H<sub>2</sub>) are generated during the low energy process of CID fragmentation in the linear ion trap (see Figure 2 for more

details). In contrast to renal sulfatides in the mice models reported by Marshing et al. [13], ceramide anchor with  $\alpha$ -hydroxyl acyl chains are often observed in human RCC tissue samples. The fragmentation pattern is similar as for the analogues with N-acyl non-hydroxylated chains except for one additional specific fragmentation arising from the cleavage of C-C bond between the carbonyl and  $\alpha$ -hydroxy carbon, as demonstrated in the fragmentation scheme of SulfoHex<sub>2</sub>Cer d18:1/24:1(OH) (Supplementary Figure S2) in the fragmentation path of *m/z* 1066–730 (NL of  $\Delta m/z$  336). The scheme of basic CID fragmentation processes together with the list of observed NL corresponding to present hydroxylated and non-hydroxylated fatty acyls of N-acyl part and sphingoid base part with two or three hydroxyls for all identified SulfoHex<sub>2</sub>Cer species are shown in Figure 3. Couple of ions are further formed by direct NL of  $\Delta m/z$  162 (C<sub>6</sub>H<sub>10</sub>O<sub>5</sub>, hexose-H<sub>2</sub>O) and 180 (C<sub>6</sub>H<sub>12</sub>O<sub>6</sub>) in MS/MS of all deprotonated molecules of dihexosylceramide sulfates (see ions at *m/z* 888 and 870 in Figure 1b). Although these NL could misleadingly indicate the sulfate position on the first hexosyl unit (closer to ceramide anchor), the opposite is true, and these ions are formed by the

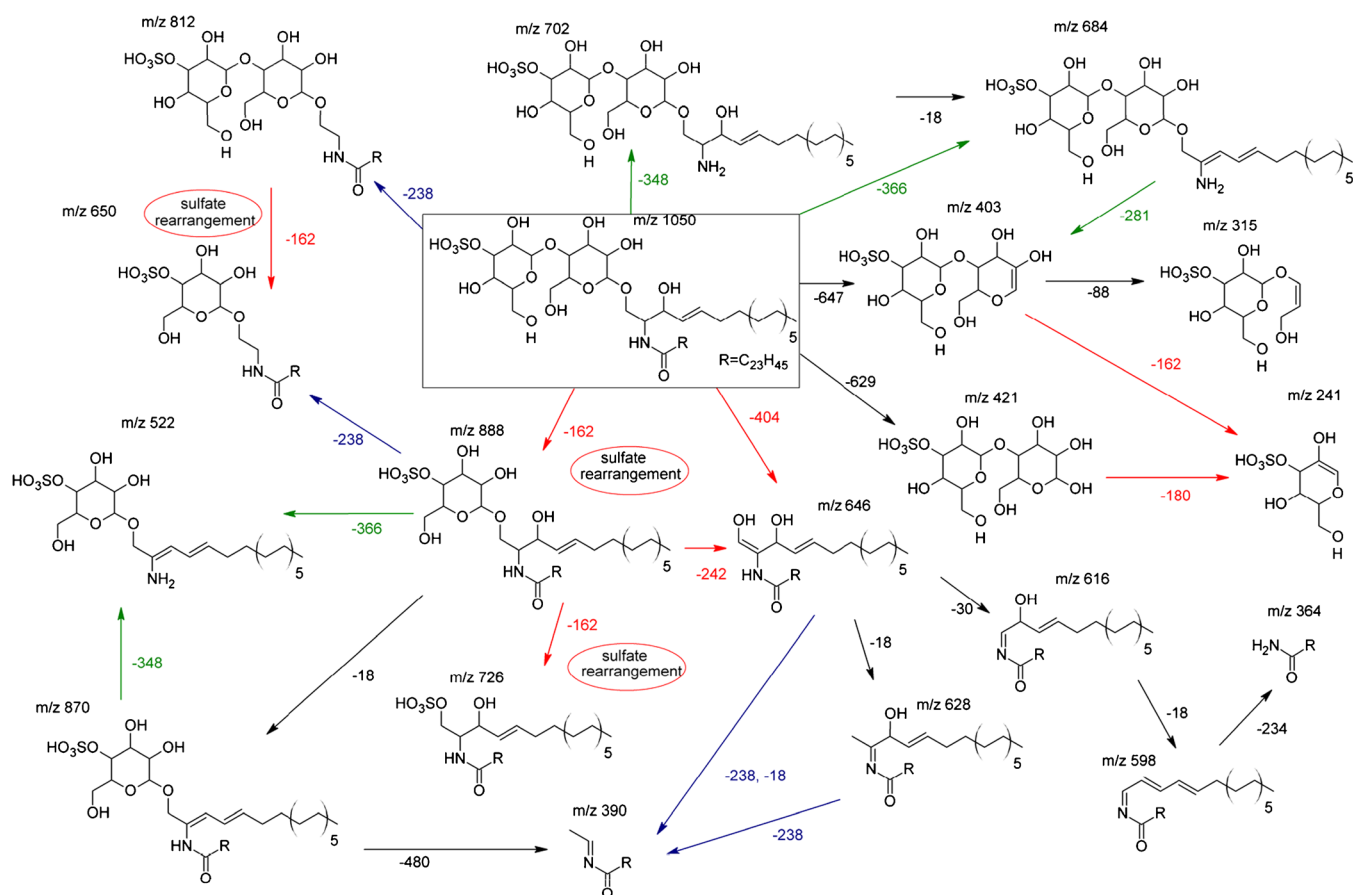


**Figure 2.** Suggested fragmentation pattern of SulfoHex<sub>2</sub>Cer d18:1/24:1 at  $m/z$  1050. The color of arrows is associated with NL of particular parts of the molecule, where red represents NL of saccharide part, green represents NL of N-acyl part, and blue represents NL of sphingoid base part. Deprotonated molecules are recorded in measured spectra for all shown structures

rearrangement process described previously for monohexosyl sulfatides [11]. This rearrangement is also observed during MS<sup>3</sup> and MS<sup>4</sup> fragmentations and even ions corresponding to particular sulfo-ceramide after two subsequent rearrangement processes were found for these compounds (see fragmentation path 1050–888 (870)–726 (708) in Figure 2). Incorrect assignment of sulfate position would provide false positive result and would be in conflict with the metabolic pathways of these compounds [39]. Particular ions presented in MS/MS of identified SulfoHex<sub>2</sub>Cer species are listed in Supplementary Table S5. The last type of fragmentation (Figure 1c), PQD, provides similar fragmentation as for CID; however, at the same time it allows the observation of low  $m/z$  fragments that are usually excluded from CID spectra and also helps to access higher energy dissociation channels [40].

#### Fragmentation of SulfoHexNAcHex<sub>2</sub>Cer, SulfoHexNAcHex<sub>3</sub>Cer, SulfoHexNAcHex<sub>4</sub>Cer

In the case of MS/MS of deprotonated molecule of SulfoHexNAcHex<sub>2</sub>Cer at  $m/z$  1227, the most abundant ion was formed after NL of  $\Delta m/z$  203 (N-acetylhexoseamine-H<sub>2</sub>O), as demonstrated in Figure 1d and Supplementary Figure S3 in the CID spectrum and the fragmentation scheme of

SulfoHexNAcHex<sub>2</sub>Cer d18:1/22:0, respectively. This prominent NL confirms an outer position of N-acetylhexoseamine unit. Another important but less abundant ion at  $m/z$  887, is formed via the NH–CO bond cleavage and additional water loss ( $\Delta m/z$  340) and confirms 22:0 N-acyl in the ceramide part. The information on d18:1 sphingoid base was obtained with the help of ion at  $m/z$  989 formed after NL of particular aldehyde ( $\Delta m/z$  238). In general, these NL (Figure 3) originated from ceramide part are present in all MS/MS of all identified sulfo glycosphingolipids containing one to five hexosyl units (Supplementary Tables S5 and S6), and they are also observed in other fragmentation paths obtained by measurements of MS<sup>n</sup> spectra, as demonstrated in fragmentation schemes of selected sulfo glycosphingolipids (Supplementary Figures S2–S5). For SulfoHexNAcHex<sub>3</sub>Cer species containing the additional hexose linked to HexNAc, typical NL of  $\Delta m/z$  365 (combined NL of  $\Delta m/z$  162 and 203) together with NL of outer hexose  $\Delta m/z$  162 and  $\Delta m/z$  180 (hexose) are observed in MS/MS, as evident in MS/MS of deprotonated molecule of SulfoHexNAcHex<sub>3</sub>Cer d18:1/24:1 at  $m/z$  1415 (Figure 1e). MS/MS of deprotonated molecules of SulfoHexNAcHex<sub>4</sub>Cer (Figure 1f) are characterized by the NL of  $\Delta m/z$  162 (180), 365, and 527. The presence of  $\Delta m/z$  365 and no NL corresponding to the loss of two hexoses provides evidence that the last hexosyl unit is probably



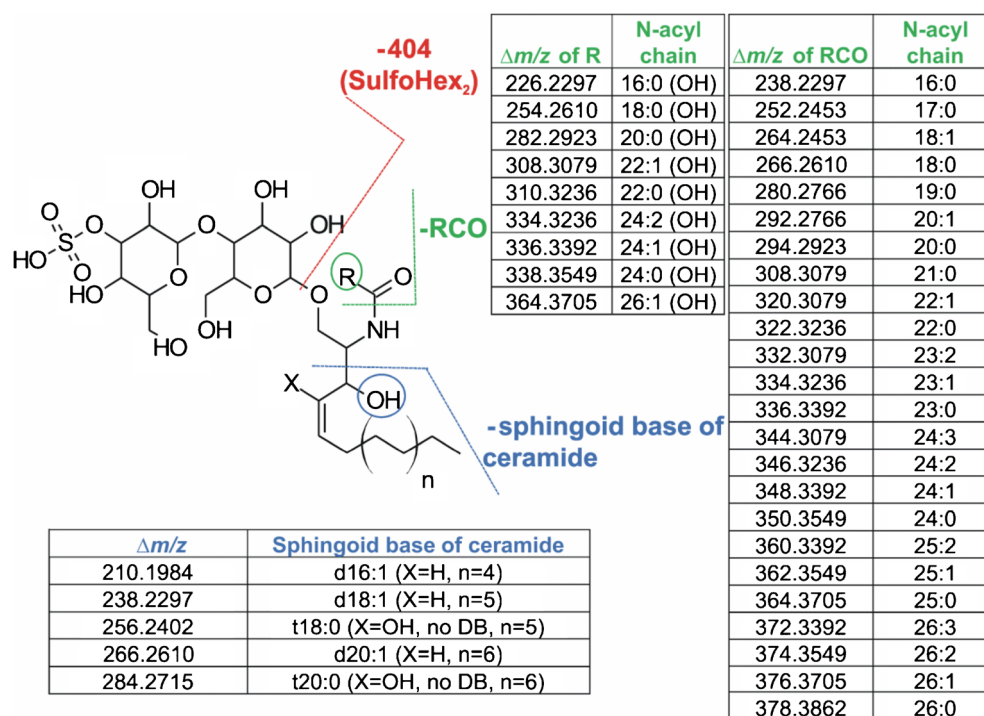


**Figure 3.** CID fragmentation process together with the list of observed NL corresponding to hydroxylated and non-hydroxylated N-acyl and sphingoid base parts for all identified SulfoHex<sub>2</sub>Cer species

linked to the first or second hexosyl unit from the side of ceramide part. Product ions associated with saccharide units are present in all MS/MS of glycosphingolipid sulfates. The cleavage of the bond between ceramide and whole saccharide part results in the formation of negatively charged ceramide and particular saccharide ions, as illustrated in Figure 1d–f, where adequate ions at  $m/z$  620 and 606 (624) for MS/MS of SulfoHexNAcHex<sub>2</sub>Cer d18:1/22:0, ions at  $m/z$  646 and 768 (786) for MS/MS of SulfoHexNAcHex<sub>3</sub>Cer d18:1/24:1, and ions at  $m/z$  646 and 930 (948) for MS/MS of SulfoHexNAcHex<sub>4</sub>Cer d18:1/24:1 are observed, respectively. Other smaller product ions of whole saccharide chain formed by the cleavage of the interglycosidic bond ( $m/z$  444, 241, and 97) are further generated in particular MS/MS during CID process. The rearrangement of sulfates described above for mono- and dihexosyl sulfates is not observed in MS/MS spectra of deprotonated molecules of their analogues with more hexosyl units, and this fragmentation process is observed only during additional MS<sup>n</sup> of their product ions that correspond to the mass of SulfoHex<sub>2</sub>Cer. This fact indicates that sulfate rearrangement is preferred for ions with sulfate position on the last hexosyl unit (Supplementary Figures S2–S5).

### MALDI-Orbitrap-MSI Experiments

MALDI-Orbitrap-MSI was further used to obtain information on the lipid composition of RCC and autologous normal tissues. Two adjacent surgically removed kidney tissue slices of selected RCC patient were cut simultaneously. The first tissue slice was subjected to histologic staining for the diagnostic evaluation of RCC and

surrounding non-affected tissues. Ion currents corresponding to  $m/z$  values of identified sulfoglycosphingolipids and other lipid species were further extracted in case of MALDI-MSI of the second tissue slice. The spatial maps were compared with the results obtained from histology with the aim to find the largest differences in lipid profiles between the two tissue parts. All MS images representing extract ion currents (EIC) of  $m/z$  values were reconstructed with mass tolerance of  $\Delta m/z$  0.005. 9-AA matrix was also used in case of MSI experiments. Long-term stability of matrix allowed measuring pictures with lateral resolution of 120  $\mu\text{m}$  with highest Orbitrap XL resolving power of 100,000 (at  $m/z$  400). Figure 4 represents a perfect correlation of MSI and histology. Visualization of particular ions was performed using the combo picture including two colors (green and red) separately used for EIC of  $m/z_1$  and  $m/z_2$ , where the color saturation expresses peak intensity. The highest elevation in RCC tissue part was observed for SulfoHex<sub>2</sub>Cer, while some other lipids, such as phospholipids of composition 36:4 were markedly decreased, as illustrated here by representative EIC of SulfoHex<sub>2</sub>Cer 42:1 at  $m/z$  1052 and PE 36:4 at  $m/z$  738. Similar results were obtained for another patient. Two separately surgically removed tumor and normal tissue parts are compared in this case (Supplementary Figure S6). A different color visualization of changes in the lipid distribution, blue to red, is applied here, where blue represents the lowest abundance and red represents the highest abundance of particular EIC of deprotonated molecules or their ratios. Visualization of changes in the lipid ratio is very useful, especially when lipids of similar structures are compared, because no further normalization to IS is necessary (see section on validation). Although sulfoglycosphingolipids are shown to be very important in



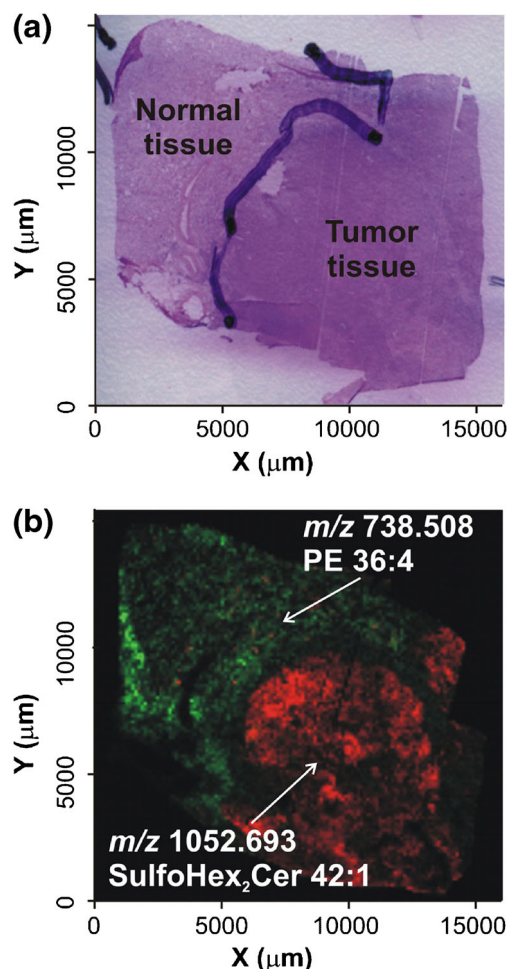


**Figure 4.** Comparison of H&E staining **(a)** with MALDI-MS imaging **(b)** of two adjacent tissue slices composed of tumor and adjacent autologous normal tissues parts. Green represents EIC of  $[\text{PE } 36:4 - \text{H}]^-$  at  $m/z$  738.508, and red represents EIC of  $[\text{SulfoHex}_2\text{Cer } 42:1 - \text{H}]^-$  at  $m/z$  1052.693

RCC metabolism based on the previous MALDI-MSI experiments, at least several dozens of patients should be analyzed to obtain statistically relevant results. However, the MALDI-Orbitrap-MS imaging of such number of patients is time-consuming in view the fact that one tissue image of  $1 \text{ cm}^2$  size of  $200 \mu\text{m}$  lateral resolution is measured approximately 3.5 h with the application of highest mass resolution and high spectra averaging to achieve reliable pictures. Thus, we decided to validate and apply classic MALDI-MS approach of matrix/tissue extract mixture measurement for this semiquantitative characterization and subsequent statistical comparison of selected lipids in tumor and autologous normal tissues of 80 RCC patients. Validation, particular statistical results, and the correlation with MALDI-MSI are described below.

#### Validation of MALDI-Orbitrap-MS Method

The principal problem of MALDI-MS quantitative analyses arises from the ionization suppression effects and heterogeneity of matrix/analyte cocrystallization during sample preparation.

Other compounds presented in the sample compete with the analyte during these processes, and the analyte of identical concentration can provide different absolute signal in the studied extracts of particular patients with regard to their biological and chemical variability (e.g., high abundance of acylglycerols is usually observed for obese patients, etc.). When compounds of interests belong to the identical lipid class (i.e., sulfoglycosphingolipids) and thus provide similar chemical and physical properties (e.g., similar behavior during extraction, cocrystallization with matrix, identical solubility, etc.), their relative abundance or changes in ratios of intensities of particular deprotonated molecules can be compared within studied RCC patients to correct for these problems and achieve acceptable semiquantitative results. Another and more common normalization is the application of IS, which should be from the same lipid class, should contain the same lipid backbone, the head group as the compound of interest, and differ only in fatty acyl chain length in order to show similar chemical and physical properties. The isotopically labeled lipids or IS with shorter fatty acyls (C12) are usually used in quantitative lipidomics and must not interfere with endogenous or matrix ions [41]. The test of selectivity proved that no interferences in close region of  $m/z$  are present (data not shown). The selectivity was followed by the measurement of calibration curve of selected IS (Supplementary Figure S7) to obtain information on the linearity range (0.37–1700 pmol/mL), LOD (0.11 pmol/mL), and LOQ (0.37 pmol/mL) values. The linearity range over three orders of magnitude with  $R^2$  greater than 0.99 proved the possibility of semiquantitation and comparison of studied sulfoglycosphingolipids in RCC tissue extracts. Among other validation parameters, carry-over effect was not observed, RSD of within-day and between-day precisions did not exceed 30%, and RSD for freeze/thaw stability was less than 20% (see Supplementary Tables S7 and S8). The matrix effect is evident from the Supplementary Table S9, where the absolute signal of internal standard is compared within 20 different RCC tissues extracts resulting in RSD 45%. Validation parameters showed that the method is applicable for semiquantitative study to find main differences in sulfoglycosphingolipid composition between tumor and autologous normal tissues. The reproducibility of spotting was calculated as the standard deviation from five consecutive spots of the sample (see particular RSD of five spots in round brackets in particular lines in Supplementary Tables S7 and S8) and it is around 10%.

#### MALDI-Orbitrap-MS Study of 80 RCC Patients

This study evaluated 80 RCC tumor and 78 adjacent normal tissue samples collected from 80 patients who underwent surgery at the University Hospital in Olomouc, Czech Republic from 2013 to 2015 (Table 1). Supplementary Figure S8 represents the flow chart of the present MALDI-MS study. Tumor and autologous normal tissues were analyzed for each patient. Each tissue is represented by one average MALDI-MS spectrum with thousands of  $m/z$  values. The automatic peak

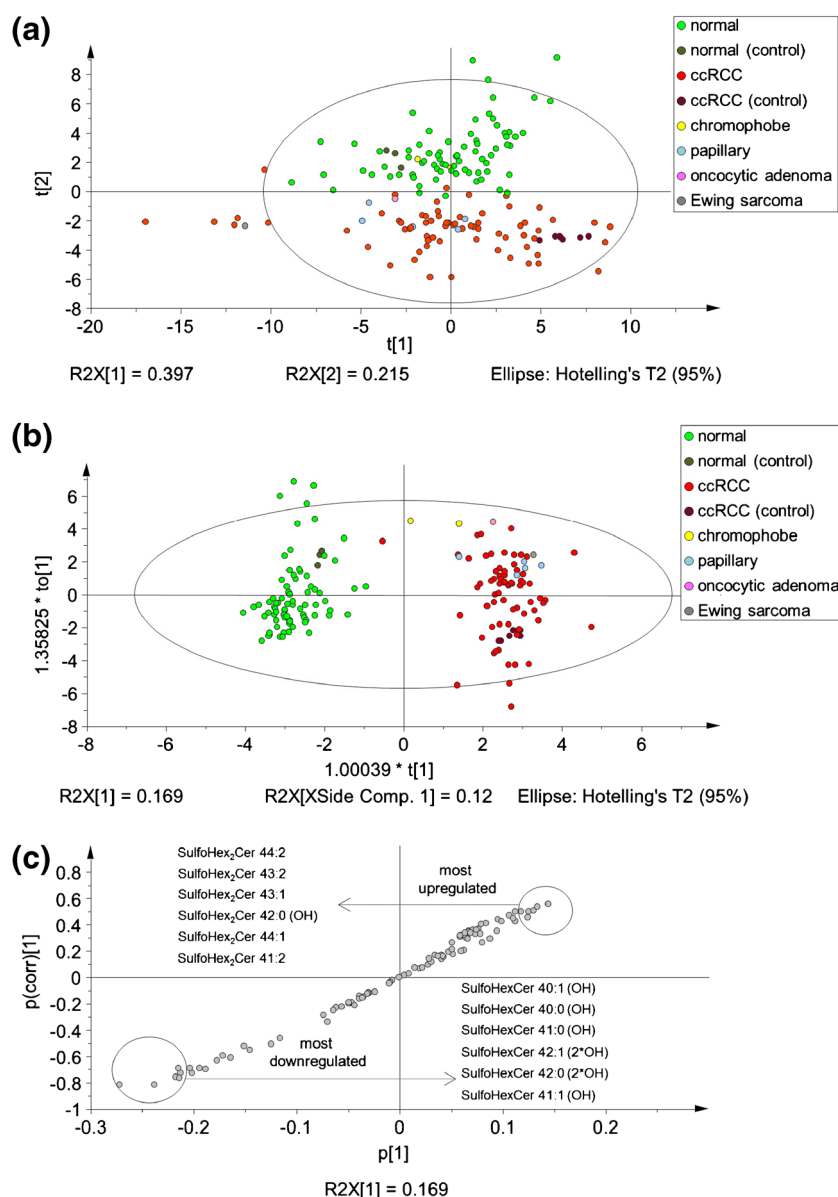


**Figure 5.** MDA of normalized intensities of sulfoglycosphingolipid species in 158 normal and tumor tissue parts of 80 RCC patients: **(a)** the score plot of unsupervised PCA method (abbreviation ccRCC means clear cell renal cell carcinoma), **(b)** the score plot, and **(c)** the S-plot of supervised OPLS-DA method

assignment is subsequently performed and particular  $m/z$  peaks are matched with deprotonated molecules from a database created during the identification procedure using the Excel macro script. This peak assignment results in the generation of the list of present  $m/z$  (illustrated here by numbers 1 to X) of studied sulfo glycosphingolipids with the average intensities (INT) in particular spectra for each 158 samples (illustrated here by capitals A to Z). The values of intensities below LOQ (minimum value of statistical confidence level) are subsequently replaced by  $2/3$  of lowest quantified value in order to unify statistically insignificant or zero values and enable further processing based on logarithmic calculations, similarly as described previously by Martin-Fernandez et al. [42]. Corrected intensities are subsequently normalized to IS or particular ratios of intensities within one lipid class are generated. Finally,

statistical evaluation and comparison of normalized data set is performed. The total acquisition time of one sample including five consecutive spots was around 10 min. The control sample should be placed at the beginning, middle, and end positions of MALDI plate within each run for later verification of signal stability. If the measurement of studied samples cannot be performed on one MALDI plate, the control sample should also be placed on another MALDI plate or identical MALDI plate after the washing step. The measurement of all 158 studied samples with five repetitions was performed within 3 d including two washing steps of MALDI plate. Two control samples were randomly selected from our sample set, and low RSD in Supplementary Table S10 show good reproducibility of relative signal for selected sulfoglycosphingolipids and demonstrate that no significant effect disrupting the measurement is

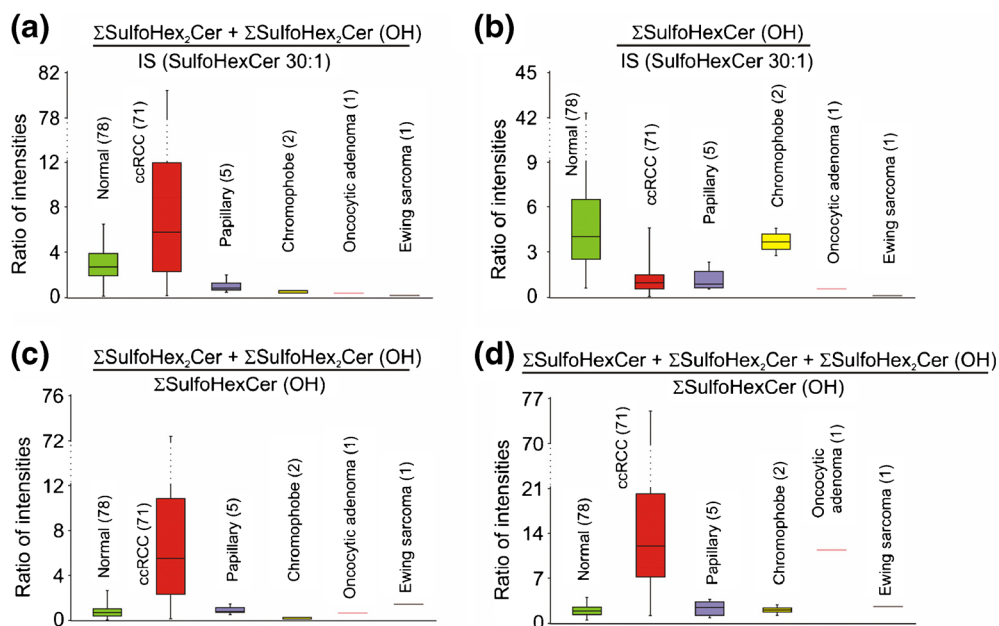


**Figure 6.** Box plots representing sum of intensities of particular lipid subclasses normalized to the internal standard or their ratios in studied 158 normal and tumor tissues of 80 RCC patients. Numbers in brackets signify number of samples of particular RCC tissue subtype

observed within 3 d of study. The RSD values in the brackets behind the average values and standard deviations inside of particular columns under each day represent the signal fluctuation within three positions (start, middle, and end) of MALDI plate (except first-day run of tissue sample 10T for which only one position was measured) and total RSD expresses total signal variation including plate positions and particular days of all three runs. The absolute signal of sulfoglycosphingolipids is related either to the intensity of used IS or to another observed sulfatide. Additional control can be subsequently done after PCA or OPLS-DA plot creation, where minimum statistical scattering should be observed for these control samples, as illustrated in Figure 5a and b. Control samples of tumor are dark red (seven points), whereas control samples from normal tissues are dark green (three points). Low statistical scattering of control samples proves the stability and reproducibility of all individual steps in the sample preparation and analysis.

### Statistical Evaluation of Normalized MALDI-Orbitrap-MS Data

MDA of normalized data of all 158 samples using unsupervised (PCA) and supervised (OPLS-DA) statistical tools was performed for the simplified visualization of most significant differences between tumor and autologous normal tissues (Figure 5). The intensities of sulfoglycosphingolipids containing more than two hexosyl units were not input for the statistical comparison because these compounds were detected only in less than 10% of studied samples, mostly in tumor tissues. Particular data points of individual tissue types are specifically colored for better visualization in score plots, where green is

used for normal, red for clear cell RCC (ccRCC), blue for papillary RCC, yellow for chromophobe RCC, pink for oncocytic adenoma, and brown for Ewing's sarcoma tissue samples. The score plot of PCA method (Figure 5a) shows a good clustering of normal and tumor tissue data points with a small degree of overlap in the region at the boundary of groups. No separation from the normal tissue samples is only observed for chromophobe RCC subtype. The first component in PCA method explains 39.7% of the variation, whereas the second component explains 21.5%. The application of supervised OPLS-DA method with predefined two groups of samples (normal versus tumor) exhibits even better group separation (Figure 5b). Lipid species responsible for separation quality of clusters are visualized in the S-plot (Figure 5c). SulfoHex<sub>2</sub>Cer 44:2, SulfoHex<sub>2</sub>Cer 43:2, SulfoHex<sub>2</sub>Cer 43:1, SulfoHex<sub>2</sub>Cer 42:0 (OH), SulfoHex<sub>2</sub>Cer 44:1, SulfoHex<sub>2</sub>Cer 41:2, SulfoHex<sub>2</sub>Cer 40:0 (OH), SulfoHex<sub>2</sub>Cer 34:2 (OH), and SulfoHex<sub>2</sub>Cer 42:3 (OH) belong among the most upregulated sulfoglycosphingolipids, whereas SulfoHexCer 41:1 (OH), SulfoHexCer 42:0 (2\*OH), SulfoHexCer, 41:0 (OH), SulfoHexCer 42:1 (2\*OH), SulfoHexCer 40:0 (OH), SulfoHexCer 40:1 (OH), SulfoHexCer 41:0 (2\*OH), and SulfoHexCer 43:1 (OH) are most downregulated in tumor tissues. The significant elevation of some non-hydroxylated SulfoHexCer, such as SulfoHexCer 42:3, SulfoHexCer 42:4, SulfoHexCer 44:3, and SulfoHexCer 40:3, is also observed in RCC tumor tissues. Box plots representing normalized intensities of selected up- and downregulated lipids or their ratios are illustrated in Supplementary Figures S9–S11, respectively. In general, the most pronounced trend in tumor tissues is upregulation of sulfoglycosphingolipids with two hexosyl units SulfoHex<sub>2</sub>Cer and SulfoHex<sub>2</sub>Cer (OH) and downregulation

of SulfoHexCer (OH), as evident from the box plots of sums of normalized intensities of particular sulfoglycosphingolipid subclasses for all histologic subtypes in Figure 6. The elevation of SulfoHex<sub>2</sub>Cer and SulfoHex<sub>2</sub>Cer (OH) is only observed in case of clear cell RCC (ccRCC), but not for other RCC subtypes. On the other hand, significant decrease of SulfoHexCer (OH) is observed in all tumor tissues with the exception of chromophobe subtype, which provides no significant differences from normal tissues (Figures 5a and 6b). These trends are corroborated by previously published reports describing enhanced activity of sulfotransferase in human RCC, as well as by the article of Kim et al. [29], where the decrease of SulfoHexCer 40:1 (OH) and SulfoHexCer 42:1 (OH) was the most significant difference between RCC tumor and autologous normal tissues. Furthermore, the MALDI-MS measurement of 80 patients shows the good correlation with MSI data described above (Supplementary Figure S6). Although, the present paper is focused mainly on the analysis of sulfoglycosphingolipids, other lipid species (SM or phospholipids) together with appropriate IS were present in measured mass spectra allowing for their normalization and comparison in studied tissue samples. The downregulation of SM 36:1, SM 38:1, PE 36:4 and PE 34:2 observed in the tumor is in agreement with recently published data obtained using hydrophilic interaction liquid chromatography coupled to electrospray MS [43].

Biomarkers play an increasingly important role in the management of cancer patients [44], but the utilization of biomarkers in RCC patients is currently limited. Although targeted therapy is the mainstay of systemic treatment in RCC, treatment strategy is based on sequential administration of another drug with known activity in the disease after the failure of prior therapy rather than a targeted approach directed by molecular biomarkers [45]. It remains to be determined in future studies whether sulfoglycosphingolipids could be useful as biomarkers in patients with this common malignancy.

## Conclusions

In this work, we have demonstrated that MALDI-Orbitrap-MS with 9-AA as matrix enables a semiquantitative comparison of sulfoglycosphingolipids in 158 tumor and autologous normal tissues of 80 RCC patients. The high sensitivity and the linearity range over 3 orders of magnitude in the negative-ion mode allows us to analyze a wide range of studied sulfoglycosphingolipids altogether in one mass spectrum. In total, 52 species for sulfoglycosphingolipids with one, 40 with two (48 for fatty acyl level), 12 with three, 5 with four, and 10 with five hexosyl units are identified in studied RCC tissue samples using high resolution full scan and tandem mass spectra measurements. Many of identified sulfoglycosphingolipids are reported here for the first time. Systematical description of gas-phase fragmentation processes for all sulfoglycosphingolipid subclasses differing in the number of hexosyl units (up to five hexosyl units) is further done with the aim to detailed structural elucidation including the composition of saccharide and ceramide parts. Significant differences in

sulfoglycosphingolipid abundances are found based on the statistical comparison of all studied RCC tumor and autologous normal tissues. The elevated levels of SulfoHexCer, SulfoHex<sub>2</sub>Cer, and SulfoHex<sub>2</sub>Cer (OH) species in tumor tissues compared to adjacent normal tissues correlate with previously described enhanced cerebroside sulfotransferase activity in RCC cells [8, 9, 28, 46]. On the other hand, the decreased concentration of SulfoHexCer (OH) is observed in agreement with the results reported by Kim et al. [29]. Sulfoglycosphingolipids, compounds with anionic extracellular charge, have been recently found to be responsible for urinary pH regulation, ammonium excretion, and play an important role in the regulation of acidobasic homeostasis [3]. It was demonstrated that the lack of renal sulfatides leads to more acidic urinary pH. On the other hand, RCC metabolism showed close association with glutamine metabolism [47] and uses glutamine as energy source resulting in the overexpression of ammonium ions. Thus, the dysregulation of sulfoglycosphingolipids can be a consequence of RCC metabolic pathways. The present MALDI-Orbitrap-MS results indicate the highest significance in the comparison of specific intensity ratio of upregulated SulfoHexCer, SulfoHex<sub>2</sub>Cer, and SulfoHex<sub>2</sub>Cer (OH) to downregulated SulfoHexCer (OH), which showed to be most powerful for tumor and autologous normal tissue differentiation, and opened the way for the investigation of sulfoglycosphingolipids role as biomarkers for early RCC diagnosis or monitoring of treatment results that could potentially aid in increasing the cure rate. We assume that these concentration changes should be also be reflected in body fluids, and thus the current research will continue with an analysis of plasma and urine of cancer patients and healthy volunteers with emphasis on dysregulated sulfoglycosphingolipids identified in tumor tissues.

## Acknowledgements

This work was supported by the ERC CZ project no. LL1302 sponsored by the Ministry of Education, Youth, and Sports of the Czech Republic. The help of Pavel Čaň and Eva Cífková with Excel macro script is greatly acknowledged.

## References

1. Ishizuka, I.: Chemistry and functional distribution of sulfoglycolipids. *Prog. Lipid Res.* **36**, 245–319 (1997)
2. Takahashi, T., Suzuki, T.: Role of sulfatide in normal and pathological cells and tissues. *J. Lipid Res.* **53**, 1437–1450 (2012)
3. Stettner, P., Bourgeois, S., Marsching, C., Traykova-Brauch, M., Porubsky, S., Nordstrom, V., Hopf, C., Kusters, R., Sandhoff, R., Wiegandt, H., Wagner, C.A., Grone, H.J.: Sulfatides are required for renal adaptation to chronic metabolic acidosis. *Proc. Natl. Acad. Sci. U. S. A.* **110**, 9998–10003 (2013)
4. Spáčil, Z., Kumar, A.B., Liao, H.C., Auray-Blais, C., Stark, S., Suhr, T.R., Scott, C.R., Tureček, F., Gelb, M.H.: Sulfatide analysis by mass spectrometry for screening of metachromatic leukodystrophy in dried blood and urine samples. *Clin. Chem.* **62**, 279–286 (2016)
5. Han, X.L., Holtzman, D.M., McKeel, D.W., Kelley, J., Morris, J.C.: Substantial sulfatide deficiency and ceramide elevation in very early Alzheimer's disease: potential role in disease pathogenesis. *J. Neurochem.* **82**, 809–818 (2002)



6. Han, X.L.: Multidimensional mass spectrometry-based shotgun lipidomics and the altered lipids at the mild cognitive impairment stage of Alzheimer's disease. *BBA- Mol. Cell Biol. Lipids* **1801**, 774–783 (2010)
7. Liu, Y., Chen, Y.F., Momin, A., Shaner, R., Wang, E., Bowen, N.J., Matyunina, L.V., Walker, L.D., McDonald, J.F., Sullards, M.C., Merrill, A.H.: Elevation of sulfatides in ovarian cancer: an integrated transcriptomic and lipidomic analysis including tissue-imaging mass spectrometry. *Mol. Cancer* **9**, 186 (2010)
8. Honke, K., Tsuda, M., Hirahara, Y., Miyao, N., Tsukamoto, T., Satoh, M., Wada, Y.: Cancer-associated expression of glycolipid sulfotransferase gene in human renal cell carcinoma cells. *Cancer Res.* **58**, 3800–3805 (1998)
9. Sakakibara, N., Gasa, S., Kamio, K., Makita, A., Koyanagi, T.: Association of elevated sulfatides and sulfotransferase activities with human renal-cell carcinoma. *Cancer Res.* **49**, 335–339 (1989)
10. Wu, X.Z., Honke, K., Zhang, Y.L., Zha, X.L., Taniguchi, N.: Lactosylsulfatide expression in hepatocellular carcinoma cells enhances cell adhesion to vitronectin and intrahepatic metastasis in nude mice. *Int. J. Cancer* **110**, 504–510 (2004)
11. Hsu, F.F., Turk, J.: Studies on sulfatides by quadrupole ion-trap mass spectrometry with electrospray ionization: structural characterization and the fragmentation processes that include an unusual internal galactose residue loss and the classical charge-remote fragmentation. *J. Am. Soc. Mass Spectrom.* **15**, 536–546 (2004)
12. Ohashi, Y., Nagai, Y.: Fast-atom-bombardment chemistry of sulfatide (3-sulfo-galactosylceramide). *Carbohydr. Res.* **221**, 235–243 (1991)
13. Marsching, C., Jennemann, R., Heilig, R., Grone, H.J., Hopf, C., Sandhoff, R.: Quantitative imaging mass spectrometry of renal sulfatides: validation by classical mass spectrometric methods. *J. Lipid Res.* **55**, 2343–2353 (2014)
14. Jirásko, R., Holčápek, M., Kuneš, M., Svatoš, A.: Distribution study of atorvastatin and its metabolites in rat tissues using combined information from UHPLC/MS and MALDI-Orbitrap-MS imaging. *Anal. Bioanal. Chem.* **406**, 4601–4610 (2014)
15. Han, M., Jun, S.H., Song, S.H., Park, H.D., Park, K.U., Song, J.: Ultra-performance liquid chromatography/tandem mass spectrometry for determination of sulfatides in dried blood spots from patients with metachromatic leukodystrophy. *Rapid Commun. Mass Spectrom.* **28**, 587–594 (2014)
16. Ikeda, K., Taguchi, R.: Highly sensitive localization analysis of gangliosides and sulfatides including structural isomers in mouse cerebellum sections by combination of laser microdissection and hydrophilic interaction liquid chromatography/electrospray ionization mass spectrometry with theoretically expanded multiple reaction monitoring. *Rapid Commun. Mass Spectrom.* **24**, 2957–2965 (2010)
17. Mirzaian, M., Kramer, G., Poorthuis, B.J.H.M.: Quantification of sulfatides and lysosulfatides in tissues and body fluids by liquid chromatography-tandem mass spectrometry. *J. Lipid Res.* **56**, 936–943 (2015)
18. Cheng, H., Sun, G., Yang, K., Gross, R.W., Han, X.L.: Selective desorption/ionization of sulfatides by MALDI-MS facilitated using 9-aminoacridine as matrix. *J. Lipid Res.* **51**, 1599–1609 (2010)
19. Kyogashima, M., Tamiya-Koizumi, K., Ehara, T., Li, G., Hu, R., Hara, A., Aoyama, T., Kannagi, R.: Rapp demonstration of diversity of sulfatide molecular species from biological materials by MALDI-TOF MS. *Glycobiology* **16**, 719–728 (2006)
20. Vermillion-Salsbury, R.L., Hercules, D.M.: 9-Aminoacridine as a matrix for negative mode matrix-assisted laser desorption/ionization. *Rapid Commun. Mass Spectrom.* **16**, 1575–1581 (2002)
21. Angel, P.M., Spraggins, J.M., Baldwin, H.S., Caprioli, R.: Enhanced sensitivity for high spatial resolution lipid analysis by negative ion mode matrix assisted laser desorption ionization imaging mass spectrometry. *Anal. Chem.* **84**, 1557–1564 (2012)
22. Marsching, C., Eckhardt, M., Grone, H.J., Sandhoff, R., Hopf, C.: Imaging of complex sulfatides SM3 and SB1a in mouse kidney using MALDI-TOF/TOF mass spectrometry. *Anal. Bioanal. Chem.* **401**, 53–64 (2011)
23. Marsching, C., Rabionet, M., Mathow, D., Jennemann, R., Kremser, C., Porubsky, S., Bolenz, C., Willecke, K., Grone, H.J., Hopf, C., Sandhoff, R.: Renal sulfatides: sphingoid base-dependent localization and region-specific compensation of CerS2-dysfunction. *J. Lipid Res.* **55**, 2354–2369 (2014)
24. Pelengarís, S., Khan, M.: *The molecular biology of cancer: A Bridge from Bench to Bedside* (2nd ed.). Wiley-Blackwell, Hoboken (2013)
25. Li, P., Znaor, A., Holcatova, I., Fabianova, E., Mates, D., Wozniak, M.B., Ferlay, J., Scelo, G.: Regional geographic variations in kidney cancer incidence rates in European countries. *Eur. Urol.* **67**, 1134–1141 (2015)
26. Petějová, N., Martínek, A.: Renal cell carcinoma: review of etiology, pathophysiology, and risk factors. *Biomed. Papers* **160**, 183–194 (2016)
27. Chow, W.H., Dong, L.M., Devesa, S.S.: Epidemiology and risk factors for kidney cancer. *Nat. Rev. Urol.* **7**, 245–257 (2010)
28. Kobayashi, T., Honke, K., Kamio, K., Sakakibara, N., Gasa, S., Miyao, N., Tsukamoto, T., Ishizuka, I., Miyazaki, T., Makita, A.: Sulfolipids and glycolipid sulfotransferase activities in human renal-cell carcinoma cells. *Br. J. Cancer* **67**, 76–80 (1993)
29. Kim, I.C., Bang, G., Lee, J.H., Kim, K.P., Kim, Y.H., Kim, H.K., Chung, J.: Low C24-OH and C22-OH sulfatides in human renal cell carcinoma. *J. Mass Spectrom.* **49**, 409–416 (2014)
30. Guideline on bioanalytical method validation. European Medicines Agency, 21 July 2011. Available at: [http://www.ema.europa.eu/docs/en\\_GB/document\\_library/Scientific\\_guideline/2011/08/WC500109686.pdf](http://www.ema.europa.eu/docs/en_GB/document_library/Scientific_guideline/2011/08/WC500109686.pdf). Accessed November 1 (2016)
31. Brown, M.V., McDunn, J.E., Gunst, P.R., Smith, E.M., Milburn, M.V., Troyer, D.A., Lawton, K.A.: Cancer detection and biopsy classification using concurrent histopathological and metabolomic analysis of core biopsies. *Genome Med.* **4**, 33 (2012)
32. The LIPID MAPS Lipidomics Gateway, Lipid Classification System. Available at: [http://www.lipidmaps.org/data/classification/LM\\_classification\\_exp.php](http://www.lipidmaps.org/data/classification/LM_classification_exp.php). Accessed November 1 (2016)
33. Liebisch, G., Vizcaino, J.A., Kofeler, H., Trottmüller, M., Griffiths, W.J., Schmitz, G., Spener, F., Wakelam, M.J.O.: Shorthand notation for lipid structures derived from mass spectrometry. *J. Lipid Res.* **54**, 1523–1530 (2013)
34. Fahy, E., Cotter, D., Sud, M., Subramaniam, S.: Lipid classification, structures, and tools. *BBA-Mol. Cell Biol. Lipids* **1811**, 637–647 (2011)
35. Schuhmann, K., Herzog, R., Schwudke, D., Metelmann-Strupat, W., Bornstein, S.R., Shevchenko, A.: Bottom-up shotgun lipidomics by higher energy collisional dissociation on LTQ orbitrap mass spectrometers. *Anal. Chem.* **83**, 5480–5487 (2011)
36. Fuchs, B., Bischoff, A., Suss, R., Teuber, K., Schurenberg, M., Suckau, D., Schiller, J.: Phosphatidylcholines and -ethanolamines can be easily mistaken in phospholipid mixtures: a negative ion MALDI-TOF MS study with 9-aminoacridine as matrix and egg yolk as selected example. *Anal. Bioanal. Chem.* **395**, 2479–2487 (2009)
37. Murphy, R.C.: *Tandem Mass Spectrometry of Lipids*. The Royal Society of Chemistry, Cambridge (2015)
38. Dayon, L., Pasquarello, C., Hoogland, C., Sanchez, J.C., Scherl, A.: Combining low- and high-energy tandem mass spectra for optimized peptide quantification with isobaric tags. *J. Proteomics* **73**, 769–777 (2010)
39. KEGG: Kyoto Encyclopedia of Genes and Genomes, Sphingolipid Metabolism. Available at: [http://www.genome.jp/dbget-bin/www\\_bget?map06000](http://www.genome.jp/dbget-bin/www_bget?map06000). Accessed November 1 (2016)
40. Schwartz, J.C., Syka, J.E.P., Quarmby, S.T.: Improving the fundamentals of MS<sup>n</sup> on 2D linear ion traps: new ion activation and isolation techniques. Proceedings of the 53rd ASMS Conference on Mass Spectrometry and Allied Topics, San Antonio, TX, June 5–9 (2005)
41. Lisa, M., Holčápek, M.: High-throughput and comprehensive lipidomic analysis using ultrahigh-performance supercritical fluid chromatography-mass spectrometry. *Anal. Chem.* **87**, 7187–7195 (2015)
42. Palarea-Albaladejo, J., Martín-Fernández, J.A.: Values below detection limit in compositional chemical data. *Anal. Chim. Acta* **764**, 32–43 (2013)
43. Cífková, E., Holčápek, M., Lisa, M., Vrána, D., Melichar, B., Študent, V.: Lipidomic differentiation between human kidney tumors and surrounding normal tissues using HILIC-HPLC/ESI-MS and multivariate data analysis. *J. Chromatogr. B* **1000**, 14–21 (2015)
44. Melichar, B.: Laboratory medicine and medical oncology: the tale of two Cinderellas. *Clin. Chem. Lab. Med.* **51**, 99–112 (2013)
45. Buchler, T., Klapka, R., Melichar, B., Brabec, P., Dusek, L., Vyzula, R., Abrahamova, J.: Sunitinib followed by sorafenib or vice versa for metastatic renal cell carcinoma data from the Czech registry. *Ann. Oncol.* **23**, 395–401 (2012)
46. Honke, K.: Biosynthesis and biological function of sulfoglycolipids. *Proc Jpn. Acad. B-Phys.* **89**, 129–138 (2013)
47. Shroff, E.H., Eberlin, L.S., Dang, V.M., Gouw, A.M., Gabay, M., Adam, S.J., Bellovin, D.I., Tran, P.T., Philbrick, W.M., Garcia-Ocana, A., Casey, S.C., Li, Y.L., Dang, C.V., Zare, R.N., Felsner, D.W.: MYC oncogene overexpression drives renal cell carcinoma in a mouse model through glutamine metabolism. *Proc. Natl. Acad. Sci. U. S. A.* **112**, 6539–6544 (2015)